Title: Predictive filtering of sensory response via orbitofrontal top-down input

Authors: Hiroaki Tsukano[1,2], Michellee M. Garcia[1,2], Pranathi R. Dandu[1,2], Hiroyuki K. Kato[1-5]*

Affiliations:

[1]Department of Psychiatry, University of North Carolina at Chapel Hill; Chapel Hill, 27599, USA.

[2]Neuroscience Center, University of North Carolina at Chapel Hill; Chapel Hill, 27599, USA.

[3]Carolina Institute for Developmental Disabilities, University of North Carolina at Chapel Hill; Chapel Hill, 27599, USA.

[4]Eaton-Peabody Laboratories, Massachusetts Eye and Ear; Boston, 02114, USA.

[5]Department of Otolaryngology - Head and Neck Surgery, Harvard Medical School; Boston, 02114, USA.

*Corresponding author. Email: hkato3@meei.harvard.edu

Abstract: Habituation is a crucial sensory filtering mechanism whose dysregulation can lead to a continuously intense world in disorders with sensory overload. While habituation is considered to require top-down predictive signaling to suppress irrelevant inputs, the exact brain loci storing the internal predictive model and the circuit mechanisms of sensory filtering remain unclear. We found that daily neural habituation in the primary auditory cortex (A1) was reversed by inactivation of the orbitofrontal cortex (OFC). Top-down projections from the ventrolateral OFC, but not other frontal areas, carried predictive signals that grew with daily sound experience and suppressed A1 via somatostatin-expressing inhibitory neurons. Thus, prediction signals from the OFC cancel out behaviorally irrelevant anticipated stimuli by generating their “negative images” in sensory cortices.

Main Text:

Throughout our lives, we are constantly exposed to a flood of sensory information from the external world. However, only a small fraction of this information reaches our conscious perception and triggers behavioral responses. This remarkable filtering, which prioritizes inputs with expected meaningful outcomes while ignoring others, arises from our brain's ability to build internal models of the world (*1–3*). These models are continuously trained through our lifetime experiences and dictate predictive relationships between sensory objects in the world. The inability to build such predictive models, and thus to apply appropriate sensory filters, is a hallmark of mental disorders such as obsessive-compulsive disorder (*4*, *5*), schizophrenia (*6*), and most notably, autism spectrum disorders (ASD)(*7–10*).

One fundamental form of such sensory filtering is habituation, the brain's ability to ignore familiar, inconsequential stimuli (*11–13*). Habituation operates through multitudes of mechanisms, allowing animals to adapt to the statistical structures of their sensory environments over a wide range of timescales. While previous research primarily focused on mechanisms for short-term plasticity lasting from milliseconds to seconds, known as "stimulus-specific adaptation" (*14–21*), habituation also extends to longer periods—days or even weeks (*22–26*)—as evidenced by the gradual reduction in our sensitivity to perfumes or traffic noise. This long-term habituation is particularly relevant for understanding the pathology of filtering deficits, as a lack of accumulated habituation to daily sensory objects throughout one's life could result in a persistently intense sensory world (*27–32*).

Contrary to the widely held belief that habituation is the "simplest form of learning," accumulating evidence has challenged this perceived simplicity. Classical internal model-free mechanisms, such as sensory receptor fatigue, homosynaptic depression, and the short-term dynamics of inhibitory neuron firing, fail to fully account for several key characteristics of habituation. These characteristics include its persistence over weeks, capacity to process complex stimuli involving multiple sensory channels,

48 context-dependence (*33–35*), and disruption by anesthesia (*36*, *37*). These observations have prompted
49 theories suggesting that habituation is associative and governed by top-down regulation informed by
50 internal models of the external world (*11*, *29*, *36*, *38*, *39*).

51 Two competing hypotheses have been proposed to explain the top-down circuit mechanisms of long-
52 term sensory habituation. The predictive negative image hypothesis posits that initially strong sensory
53 responses are gradually canceled as the top-down predictive signal grows (Fig. 1A, left, and fig. S1A).
54 Supporting this hypothesis, somatostatin-expressing inhibitory neurons (SST cells) in sensory cortices
55 increase their sensory responses over days of stimulus exposure (*40–42*), providing neuronal substrates
56 for the generation of a 'negative image' of the stimulus. An alternative is the novelty (or prediction
57 error) hypothesis, which assumes that sensory-evoked activity is weak by default and is amplified by a
58 top-down novelty signal upon the animal's first encounter with a stimulus (Fig. 1A, right)(*43–46*). This
59 view proposes that the activation of vasoactive intestinal peptide-expressing inhibitory neurons (VIP
60 cells) by the novelty signal disinhibits pyramidal neurons, and habituation occurs as the novelty signal
61 wanes over time.

62 Despite their fundamentally distinct mechanisms, activity measurements in sensory cortices alone
63 have failed to differentiate these hypotheses. Due to the reciprocal connections between SST and VIP
64 cells, both models predict similar neuronal dynamics during habituation: an increase in SST cell activity
65 and a decrease in VIP and pyramidal cell activity. To discriminate between these theories, we sought to
66 identify the source of the top-down input to A1 during daily sensory habituation and determine the
67 'default' sensory responses by removing the top-down signal.

68 **A1 neurons show sound-specific habituation across days**

69 We induced sensory habituation in awake, head-fixed mice through repeated exposure to tones over five
70 days (5–9 seconds pure tones, 7–16 seconds inter-trial interval, 70 dB SPL, 200 trials/day) (Fig. 1, B and

71 C). To track the activity of the same A1 layer 2/3 (L2/3) neural ensembles across days, we conducted
72 chronic two-photon calcium imaging. We first located A1 by intrinsic signal imaging (*47*) and virally
73 expressed GCaMP6s in the A1 of wild-type or VGAT-Cre × Ai9 mice. Three weeks after virus injection
74 and optical window implantation, we recorded sound-evoked activities from 5,483 L2/3 neurons in 20
75 mice. We chose a fixed tone frequency for each mouse and imaged the corresponding tonotopic domain
76 in A1, where we tracked the same neural ensembles throughout the experiment. Across days of sound
77 exposure, we observed clear habituation in tone responses, characterized by reduced excitation and
78 increased suppression in a sound-specific manner (Fig. 1, D to H, fig. S2, A to C, and fig. S3), consistent
79 with previous studies (*40*, *41*). Given indistinguishable results between experiments imaging all L2/3
80 neurons and those imaging only $VGAT^{-}$ pyramidal neurons, data from both experiments were combined
81 and treated as A1 pyramidal cells (fig. S2, D to G).

82 We observed two timescales of habituation: within-day habituation, which repeated daily across
83 trials, and across-day habituation, which built up over multiple days (Fig. 1, I and J). To better
84 understand the relationship between these plasticity timescales, we projected high-dimensional
85 population dynamics onto the axes defined by within-day and across-day changes. Notably, these two
86 habituation mechanisms represented nearly orthogonal axes in the high-dimensional space (78.2 degree;
87 Fig. 1K), indicating that across-day habituation is not simply the accumulated effect of within-day
88 habituation. Within-day habituation markedly attenuated sound onset responses, whereas across-day
89 habituation was greater during the sustained phase of tones (5 seconds after onset), implying two
90 independent mechanisms for auditory habituation (Fig. 1, G, L, and M, and Supplementary Text). This
91 difference in kinetics supports the role of slow, top-down predictive filtering in across-day habituation,
92 while within-day habituation may be driven by faster, bottom-up mechanisms.

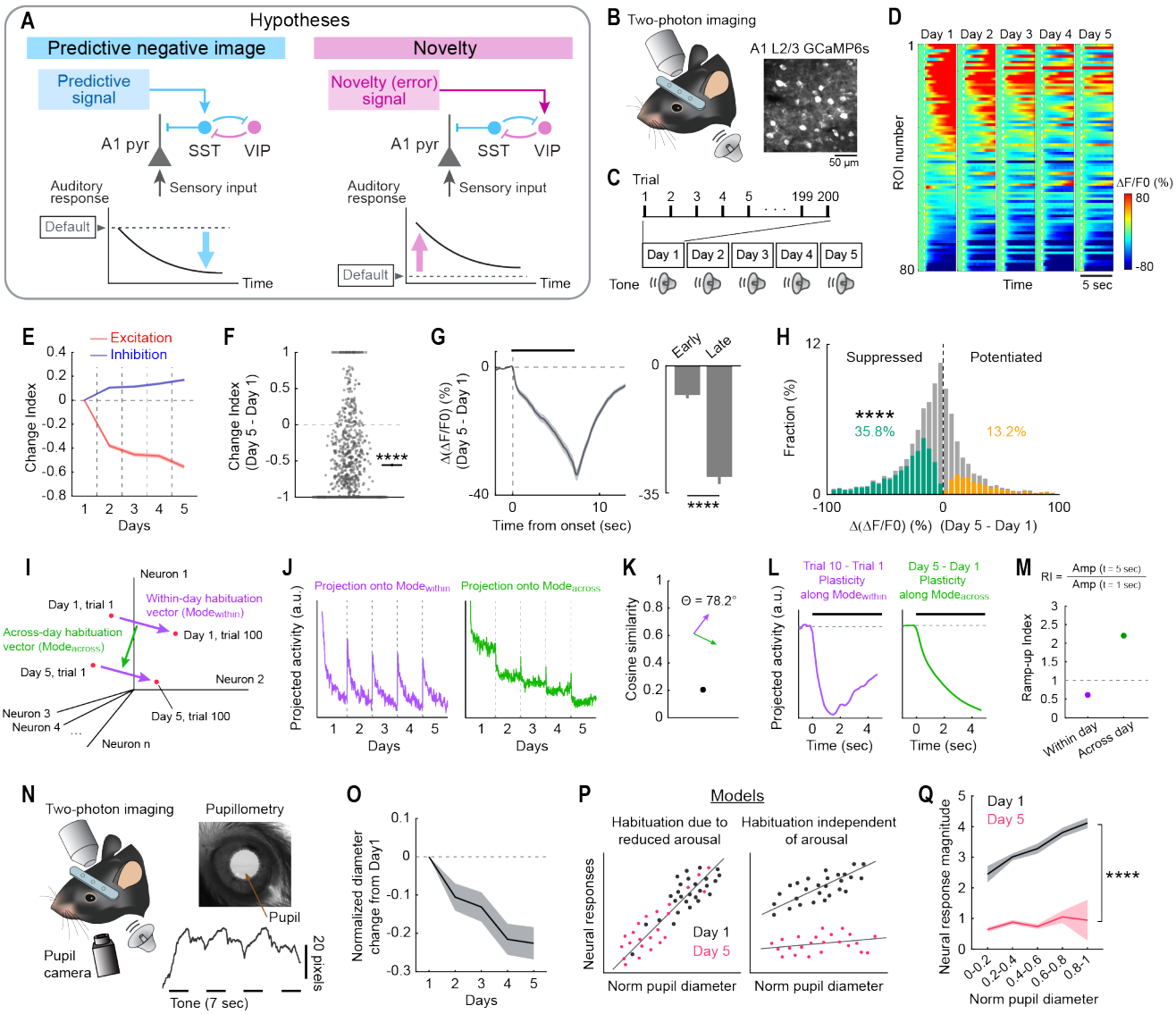

Fig. 1. Inactivation of OFC reverses across-day habituation in A1. (**A**) Schematics illustrating two theories explaining sensory habituation by top-down predictive mechanisms. (**B**) Representative two-photon image of A1 L2/3 neurons expressing GCaMP6s. (**C**) Schematic illustrating the five-day auditory habituation paradigm. (**D**) Heatmaps of sound-evoked responses in neurons imaged across five days in a representative mouse. Neurons are sorted by their responses on Day 1. (**E**) Average (solid line) and SEM (shading) of the Change Index for excitatory (red) and inhibitory (blue) sound-evoked responses across days. n = 20 mice. (**F**) Change Index of excitatory responses in individual neurons on Day 5 compared to Day 1 across all mice. Black lines on the right represent mean ± SEM. n = 879 responsive neurons. ****$P = 1.6 \times 10^{-66}$ (two-sided Wilcoxon signed-rank test). (**G**) Left: Change in sound-evoked response traces from Day 1 to Day 5 averaged across all significantly excited cells. Black bar: sound. Right: The amplitudes of the difference trace at 1 and 7 seconds after sound onset. ****$P = 1.4 \times 10^{-65}$ (two-sided Wilcoxon signed-rank test). (**H**) Histograms of changes in response magnitudes in all neurons. Orange and green bars show neurons with significant increase and decrease. ****$P = 4.3 \times 10^{-138}$ (Fisher's exact test). (**I**) Schematic illustrating vectors representing within-day habituation (purple: $\text{Mode}_{\text{within}}$) and across-day habituation (green: $\text{Mode}_{\text{across}}$) within

a high-dimensional space. Each dimension corresponds to the response magnitudes of individual neurons. (**J**) Projection of trial-to-trial sound-evoked A1 ensemble activity dynamics onto the $\text{Mode}_{\text{within}}$ (left) and $\text{Mode}_{\text{across}}$ (right) vectors. Data points represent individual trials (100 trials × 5 days). Ensemble activity patterns repeated fast daily plasticity along the $\text{Mode}_{\text{within}}$ axis, while they show continuous slow plasticity along the $\text{Mode}_{\text{across}}$ axis across five days. n = 20 mice, 2,398 cells imaged throughout the five days. (**K**) Cosine similarity between $\text{Mode}_{\text{within}}$ and $\text{Mode}_{\text{across}}$, indicating a nearly orthogonal relationship. (**L**) Left: Change in sound-evoked ensemble activity along $\text{Mode}_{\text{within}}$ from Trial 1 to Trial 10, demonstrating prominent within-day, across-trial habituation around the tone onset. Right: Change in sound-evoked ensemble activity along $\text{Mode}_{\text{across}}$ from Day 1 to Day 5. Across-day habituation slowly ramps up during the sustained tone. (**M**) Summary data showing the Ramp-up Index for across-day plasticity (Day 1 to Day 5) and within-day plasticity (Trial 1 to Trial 10). (**N**) Top left: Schematic illustrating pupil monitoring during two-photon calcium imaging. Top right: Representative image from a pupil camera. Bottom right: Representative pupil diameter dynamics during sound presentations. Black lines indicate tone timings. (**O**) Change in normalized pupil diameter from Day 1. n = 17 mice. (**P**) Two alternative models illustrating the dependence of neuronal sound responses on normalized pupil diameter. Left: A model in which neuronal habituation depends on the decrease in arousal level. Right: A model in which neuronal habituation is independent of arousal level. Individual dots represent trials. Black: Day 1 trials. Red: Day 5 trials. Lines indicate regression lines. (**Q**) Experimental data showing neuronal response magnitudes binned by normalized pupil diameter separately for Day 1 (black) and Day 5 (red). Day 5 neuronal responses are smaller than Day 1 responses regardless of normalized pupil diameter. Day 1 vs. Day 5: ****$P = 2.0 \times 10^{-30}$ (unbalanced two-way ANOVA).

To assess the contribution of global neuromodulation to sensory habituation, we monitored pupil diameter during calcium imaging in a subset of experiments. Pupil diameter showed a gradual decrease across days, providing evidence of habituation in arousal responses (Fig. 1, N and O). However, two observations argued against the possibility that the A1 neuronal habituation stemmed from a general decrease in responsiveness due to lowered arousal. First, plots of trial-to-trial variability of neural activity against pupil diameter showed a distinct separation between Day 1 and Day 5 data regardless of pupil diameter, demonstrating that across-day habituation is independent of arousal levels (Fig. 1, P and Q). Second, independent calcium imaging using two different tone frequencies confirmed the sound specificity of A1 sensory habituation (fig. S3). These data suggest that sensory habituation in A1 is due to sound-specific plasticity rather than global brain state changes. Additionally, we previously found that across-day habituation under these conditions is not inherited from subcortical pathways, as the plasticity was evident in L2/3 but not in the input layer, L4 (*40*). Therefore, we focused on across-day

habituation for the rest of our analyses to determine its cortical circuit mechanisms.

Both the predictive negative image hypothesis and the novelty hypothesis involve the active recruitment of inhibitory neurons during habituation. Since VIP cell activity had not been previously monitored in A1 during across-day habituation, we performed cell type-selective calcium imaging of three inhibitory neuron subclasses—SST cells, VIP cells, and parvalbumin-expressing neurons (PV cells)—to determine their dynamics over five days. We targeted GCaMP6s to each cell type by injecting a conditional GCaMP6s-expressing virus in Cre transgenic mice. Throughout the five-day sound exposure, L2/3 VIP and PV cells exhibited neural habituation similar to pyramidal cells (fig. S4). Interestingly, SST cells showed clear heterogeneity (*48*); deep (>200 μm from the surface) SST neurons showed habituation similar to pyramidal cells, while superficial (<200 μm) neurons exhibited the opposite pattern (*40*, *41*). These findings suggest the involvement of the superficial SST cells in sensory habituation, consistent with the inhibitory dynamics proposed in both theories. However, they do not conclusively support one hypothesis over the other, prompting further investigation into the modulation source for A1 inhibitory neurons.

OFC inactivation reverses sensory habituation in A1

We therefore sought to identify the source of top-down input regulating A1 neuronal activity (Fig. 2A). First, we performed anatomical tracing. After mapping auditory cortices with intrinsic signal imaging, we injected a retrograde tracer into A1 L2/3 (Fig. 2B). Consistent with previous studies, we found many presynaptic neurons in the OFC (*49–52*), secondary motor cortex (M2)(*53–55*), and anterior cingulate cortex (ACC)(*56*) (Fig. 2, C and D), with the ventrolateral and lateral OFC (hereafter, jointly called OFCvl) showing the densest inputs. The lack of overlap between the tracer and VGAT expression indicated that the top-down projections from OFCvl were glutamatergic (fig. S5, A to D). Cell type-selective retrograde tracing with rabies virus further confirmed that both SST and VIP cells receive

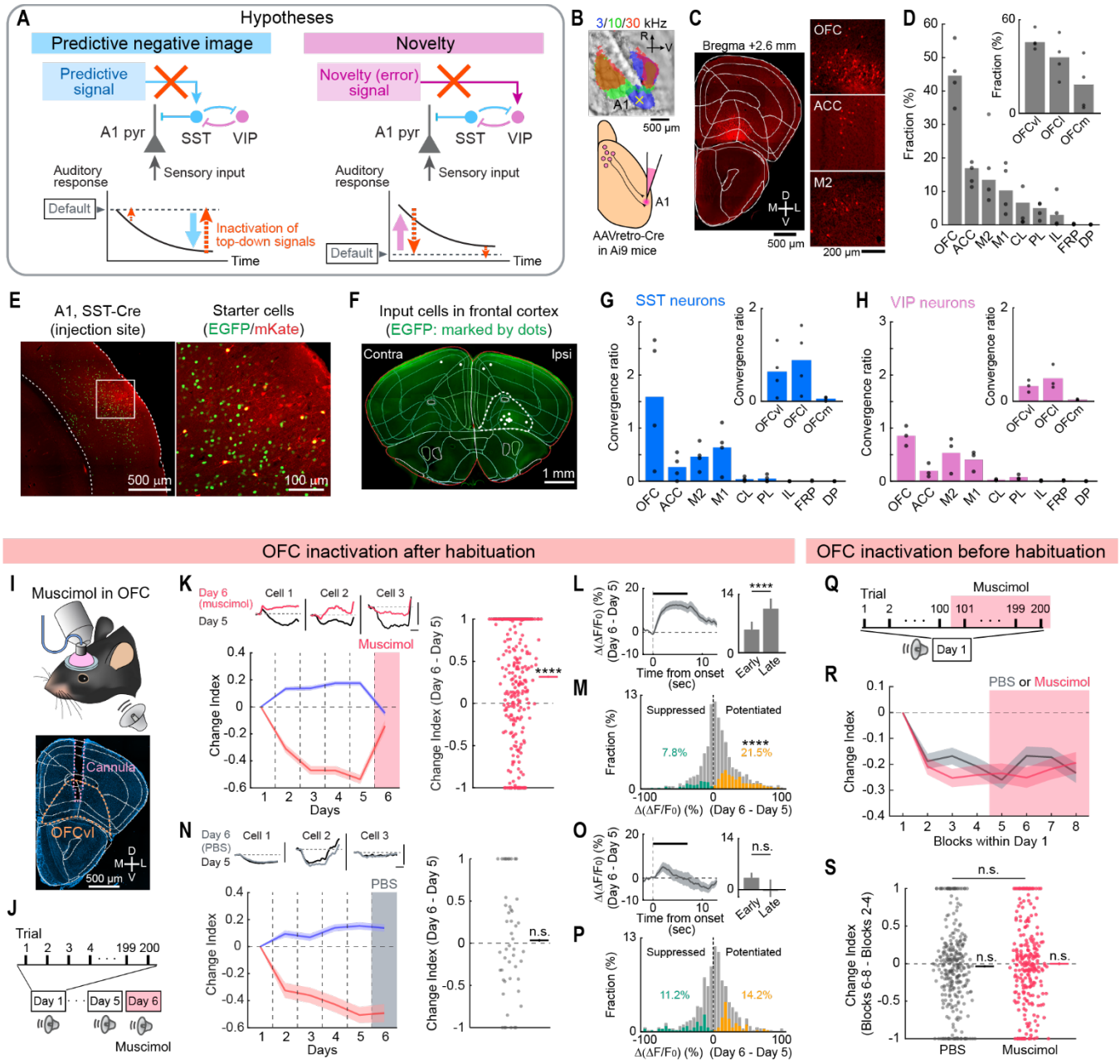

Fig. 2. Inactivation of OFC reverses across-day habituation in A1. (**A**) Schematics illustrating two theories explaining how to distinguish top-down predictive mechanisms from novelty mechanisms. (**B**) Top: Intrinsic signal imaging of pure tone responses superimposed on the cortical surface imaged through the skull. Yellow cross: injection site. Bottom: Schematic illustrating retrograde tracing from A1 L2/3. (**C**) tdTomato-expressing input neurons onto A1 L2/3. Left: Coronal section of the frontal areas overlaid with area borders. Right: Magnified images of OFC, ACC, and M2 areas. (**D**) Bar plots summarizing the distribution of input cells in ipsilateral frontal cortical areas. M1: primary motor cortex, CL: claustrum, DP: dorsal peduncular area. Inset: Further classification of OFC into ventrolateral (OFCvl), lateral (OFCl), and medial (OFCm) subdivisions. *n* = 4 mice. (**E-G**) Retrograde tracing from A1 L2/3 pyramidal neurons using SST-Cre mice. (**E**) Left: Coronal section of the injection site in A1. Dotted lines: cortical borders. Right: Magnified view

of the area indicated by a square in the left image. (**F**) Coronal section of the frontal areas overlaid with area borders. White dots: presynaptic neurons. (**G**) Bar plots summarizing the distribution of input cells in ipsilateral frontal cortical areas. *n* = 4 mice. Inset: Further classification of OFC into ventrolateral (OFCvl), lateral (OFCl), and medial (OFCm) subdivisions. (**H**) Same as (G) but for VIP-Cre mice. (**I**) Top: Schematic illustrating muscimol infusion. Bottom: DAPI-counterstained coronal section showing the cannula implantation site in OFC. (**J**) Protocol for muscimol infusion after habituation. (**K**) Top left: Trial-averaged sound-evoked response traces from three cells. Bottom left: Change Index across days. Pink shade: Muscimol infusion. *n* = 7 mice, 1,392 neurons. Right: Change Index of excitatory responses in individual neurons on Day 6 compared to Day 5 across all mice. *n* = 296 significantly excited neurons. ****$P = 7.9 \times 10^{-16}$ (two-sided Wilcoxon signed-rank test). (**L**) Left: Change in sound-evoked response traces from Day 5 to Day 6, averaged across all significantly excited cells. Right: The amplitudes of the difference trace at 1 and 7 seconds after sound onset. ****$P = 3.4 \times 10^{-7}$. (**M**) Histograms of changes in response magnitudes in all neurons. ****$P = 5.7 \times 10^{-25}$. (**N-P**) The same as (K-M), but for control PBS infusion experiments. (**N**) *n* = 3 mice, 482 total neurons, 49 significantly excited neurons. *P* = 0.52. (**O**) *P* = 0.23. (**P**) *P* = 0.19. (**Q**) Schematic illustrating muscimol infusion in naïve mice. (**R**) Change Index for excitatory responses across blocks of trials. Each data point represents a block of 25 trials. Red: muscimol (*n* = 4 mice). Dark gray: PBS control (*n* = 6 mice). (**S**) Change Index of excitatory responses in individual neurons in blocks 6–8 compared to blocks 2–4 across all mice. *n* = 301 and 242 significantly excited neurons for PBS and muscimol. PBS: *P* = 0.67 (two-sided Wilcoxon signed-rank test), muscimol: *P* = 0.23, PBS vs. muscimol: *P* = 0.49 (two-sided Wilcoxon rank-sum test).

extensive top-down inputs from OFCvl (Fig. 2, E to H, and fig. S6; see Discussion). In contrast, tracer signals in adjacent areas, such as the frontal pole (FRP), prelimbic area (PL), and infralimbic area (IL), were weaker in both AAV and rabies tracing, indicating highly specific wiring of auditory circuits in the frontal cortex (*57–59*).

We next asked whether the frontal top-down input causally contributes to A1 sensory habituation. Two hypotheses predict distinct outcomes with the removal of top-down input (Fig. 2A, red dotted arrows). According to the predictive negative image model, removing the predictive signal should increase sensory responses following habituation but have minimal impact on naïve animals. Conversely, the novelty model suggests that eliminating the novelty signal would diminish sensory responses in naïve animals but have little effect after habituation. To test these predictions, we targeted the OFCvl for pharmacological inactivation, given its strongest top-down connection to A1. After five days of tone habituation, we inactivated OFCvl on Day 6 by infusing muscimol through a pre-implanted

208 cannula (2.5 mg/mL, 500 nL, 100 nL/min) (Fig. 2, I and J). Remarkably, OFCvl inactivation reversed
209 the sensory habituation in A1 pyramidal cells by enhancing excitatory responses and reducing
210 suppression responses, an effect not observed with the control PBS infusion (Fig. 2, K to P, and fig. S7)
211 (Change Index from Day 5 to Day 6, muscimol: 0.31 ± 0.04, $P = 7.9 \times 10^{-16}$; control: 0.034 ± 0.094, $P =$
212 0.52). In a separate experiment, we evaluated the effects of OFCvl inactivation in naïve animals by
213 infusing muscimol on Day 1 (Fig. 2Q). Unlike the post-habituation inactivation, OFCvl inactivation
214 prior to habituation did not alter tone responses (Fig. 2, R and S) (Change Index before and after
215 infusion, muscimol: -0.002 ± 0.017, $P = 0.23$; control: -0.037 ± 0.015, $P = 0.67$). The absence of
216 enhanced responses by muscimol in naïve animals rules out the role of OFCvl in transmitting novelty
217 signals or modulating general sensory processing in A1. Instead, our findings demonstrate the causal
218 role of the OFC specifically in the expression of long-term sensory habituation, aligning with the
219 predictive negative image hypothesis.

220 Given the involvement of specific inhibitory neuron subtypes in both hypotheses, we further
221 assessed whether inhibitory neurons follow the predictions of these models. We repeated the same six-
222 day OFCvl inactivation experiment while performing cell type-selective imaging of SST, VIP, and PV
223 cells (Fig. 3A). Upon OFCvl inactivation in habituated mice, sound responses in SST cells were
224 significantly reduced (Change Index from Day 5 to Day 6, -0.50 ± 0.06, $P = 1.6 \times 10^{-9}$), as expected
225 from the predictive negative image hypothesis (Fig. 3, B to E). In contrast, both VIP and PV cells
226 showed a marked enhancement in their sound responses, consistent with the release from SST cell-
227 mediated inhibition (PV: 0.18 ± 0.06, $P = 0.036$; VIP: 0.55 ± 0.10, $P = 0.0012$) (Fig. 3, F to M, and fig.
228 S7). These findings further support that the predictive signals from the OFC activate SST cells to
229 suppress other A1 cell types after habituation.

230 Interestingly, while the effects of both sensory habituation (Fig. 1, G, L, and M) and OFCvl

inactivation (Fig. 2, L, Fig. 3, D, H, and L, and fig. S7, E and F) were evident at sound onset (0–1 sec from the tone start), they were significantly more pronounced during the sustained sound stimulus. This slow kinetics of sensory habituation aligns with the recruitment of a long-distance top-down feedback loop and supports the role of prediction, as the sustained phase of the sound is more predictable than the onset.

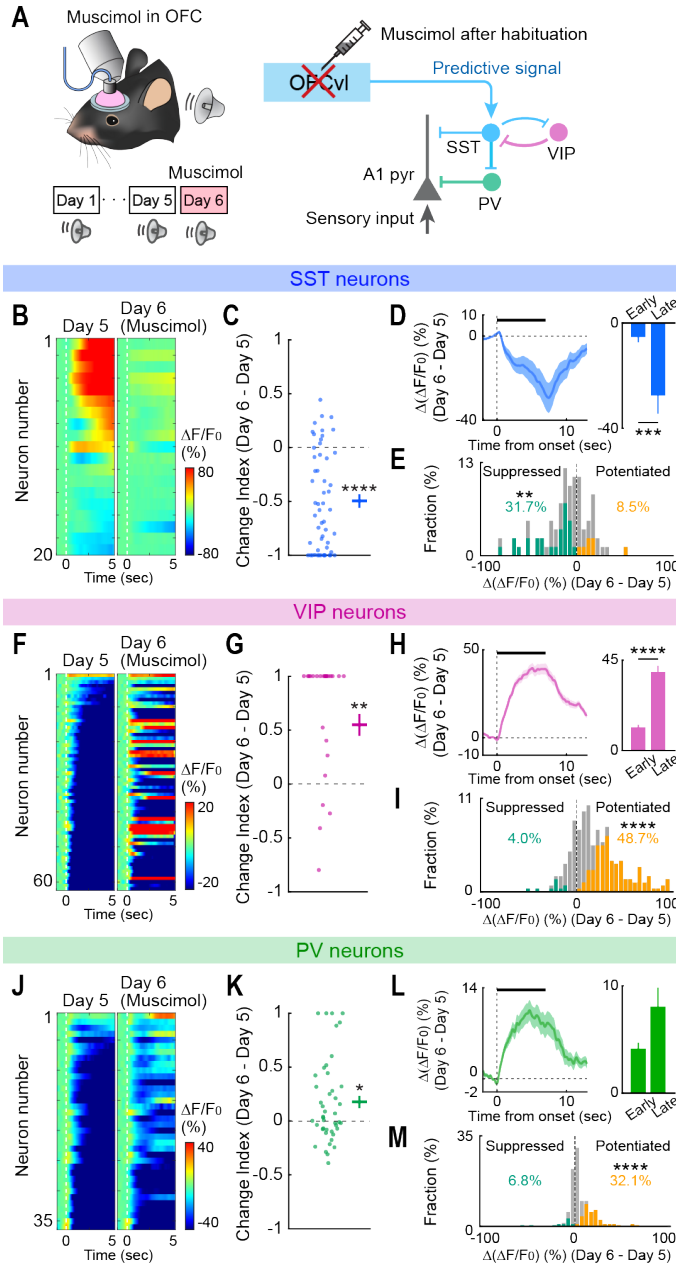

Fig. 3. Post-habituation inactivation of OFC suppresses SST neuron activity in A1. (**A**) Left: Schematic illustrating muscimol infusion after habituation. Right: Circuit diagram of inhibitory neuron connectivity in A1. (**B**) Heatmaps of sound-evoked responses in SST neurons imaged across Days 5 and 6 in a representative mouse. Neurons are sorted by their responses on Day 5. (**C**) Change Index of excitatory responses in individual SST neurons on Day 6 compared to Day 5 across all mice. Lines on the right represent mean ± SEM. n = 4 mice, 54 excited cells. ****P = 1.6 × 10^{-9} (two-sided Wilcoxon signed-rank test). (**D**) Left: Change in sound-evoked response traces from Day 5 to Day 6 averaged across all significantly excited SST cells. Solid line: average. Shading: SEM. Bar, sound. Right: The amplitudes of the difference trace at 1 and 7 seconds after sound onset. ***P = 4.7×10^{-4} (two-sided Wilcoxon signed-rank test). (**E**) Histograms of changes in response magnitudes in all SST neurons. Orange and green bars show neurons with significant increase and decrease. **P = 0.0039 (Fisher's exact test). (**F-I**) Same as (B-E) but for VIP neurons. (**G**) n = 4 mice, 26 excited cells. **P = 0.0012 (**H**) ****P = 3.3 × 10^{-26}. (**I**) ****P = 3.3 × 10^{-36}. (**J-M**) Same as (B-E) but for PV neurons. (**K**) n = 5 mice, 90 excited cells. ****P = 7.9 × 10^{-6}. (**L**) P = 0.30. (**M**) ****P = 4.2 × 10^{-5}.

236 **OFC top-down projection conveys predictive signals and suppresses A1**

237 The OFC plays critical roles in various cognitive functions and has extensive connections with multiple
238 brain regions, including the mediodorsal thalamus, striatum, amygdala, ACC, insular cortex, and sensory
239 cortical areas (*60*). We next investigated whether the direct projection from OFCvl to A1 (fig. S5, E to
240 H) conveys predictive signals during sensory habituation (Fig. 4A).

241 We visualized sound-evoked activity in the OFCvl→A1 direct pathway by virally expressing
242 axonGCaMP6s in OFCvl neurons. We performed two-photon calcium imaging of their axon terminals in
243 L1 and superficial L2/3 of A1 to track the activity from the same axon boutons over a five-day
244 habituation period (Fig. 4B). On Day 1, significant tone-evoked excitation was observed in 5.5% of
245 axon boutons, consistent with the significant but sparse sound responses previously reported in OFC of
246 naïve mice (*49*, *61*) (Fig. 4, C and D). The sound responses are likely conveyed through the anatomical
247 projections from the auditory cortex to the OFCvl (fig. S5, I to O). However, following habituation, the
248 proportion of excited boutons more than doubled to 13.2%. In axon boutons identified across days, we
249 observed a gradual increase in response magnitudes (Fig. 4, C and E). This increase in OFCvl→A1
250 axonal activity was more pronounced during the sustained phase of tones (Fig. 4F), consistent with the
251 slow kinetics of habituation in A1 neurons (Fig. 1G, and Fig. 3, D, H, and L). Moreover, this plasticity
252 was specific to the habituated tone frequency, ruling out a general increase in OFCvl responsiveness
253 (Fig. 4, G and H). These results support the hypothesis that the OFC gradually forms an internal model
254 of repeated stimuli, and its direct projection to A1 carries predictive signals that grow over days to
255 recruit SST inhibitory neurons.

256 Next, we examined whether the increase in the representation of habituated sounds is specific to the
257 OFCvl. Previous research found predictive filtering of A1 responses to self-generated sounds by
258 M2→A1 top-down input (*53–55*). Thus, predictive filtering of sensory responses may be a general

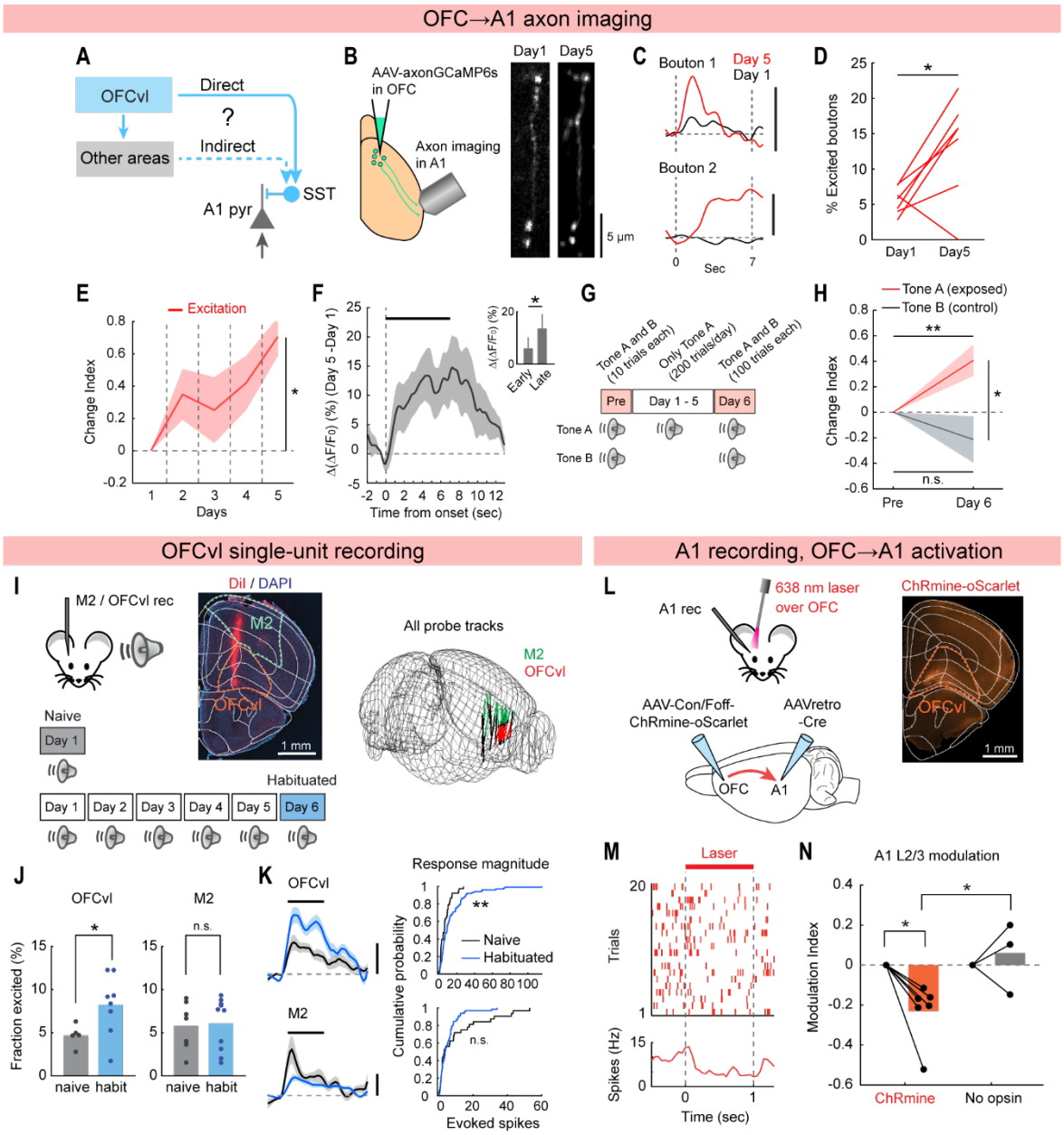

Fig. 4. OFC top-down projection conveys predictive signals and suppresses A1. (**A**) Schematic illustrating direct and indirect pathways from OFC to A1. (**B**) Left: Schematic illustrating projection-specific calcium imaging of the OFC→A1 direct pathway. Right: Representative two-photon image of a GCaMP6s-expressing OFC axon in A1 on Day 1 and Day 5. (**C**) Trial-averaged sound-evoked response traces from two axon boutons. Black: Day 1. Red: Day 5. Scale bar: 50% ΔF/F. Dotted lines indicate sound onset and offset. (**D**) Fraction of boutons with significant excitatory responses on Day 1 and Day 5 across mice. n = 7 mice, 326 boutons. *P = 0.039 (two-sided Wilcoxon signed-rank test). (**E**) Average (solid line) and SEM (shading) of the Change Index for excitatory responses across days. *P = 0.016 (Day 1 vs. Day 5, two-sided Wilcoxon signed-rank test) (**F**) Change in sound-evoked response traces from Day 1 to Day 5 averaged across all significantly excited boutons. Black bar: sound. Inset shows the amplitudes of the difference trace at 1 and 7 seconds after sound onset. *P = 0.044 (two-sided Wilcoxon signed-rank test). (**G**) Schematic illustrating the

sound-specific habituation paradigm using two sound frequencies. (**H**) Change Index of excitatory responses to Tone A (habituated) and Tone B (control) on Day 6 compared to the pre-habituation block. *n* = 7 mice, 18 and 13 significantly excited boutons for tones A and B. Tone A: ***P* = 0.0046 (two-sided Wilcoxon signed-rank test, Tone B: *P* = 0.20, Tone A vs. B: **P* = 0.025 (two-sided Wilcoxon rank-sum test). (**I**) Left: Schematic illustrating single-unit recordings in M2 and OFC of naïve and habituated mice. Middle: Coronal section showing the Neuropixels probe track (indicated by DiI) targeting M2 and OFC. The section was counter-stained with DAPI and overlaid with area borders. Right: Summary of all penetrations aligned to the Allen Common Coordinate Framework. Probe tracks within M2 and OFC are shown in green and red, respectively. *n* = 20 penetrations in 17 mice. (**J**) Fraction of single units in OFCvl (left) and M2 (right) with significant excitatory responses in naïve and habituated mice. OFCvl naïve: *n* = 5 mice, habituated: *n* = 7 mice, **P* = 0.045. M2 naïve: *n* = 7 mice, habituated: *n* = 10 mice, *P* = 0.83 (two-sided Wilcoxon rank-sum test). (**K**) Left: Sound-evoked response traces averaged across all significantly excited single units in OFCvl (top) and M2 (bottom) of naïve (black) and habituated (blue) mice. Right: Cumulative plots of sound-evoked spike counts in all significantly excited single units for OFCvl (top) and M2 (bottom). OFCvl, naïve: n = 38 units, habituated: n = 99 units, ***P* = 0.010. M2, naïve: *n* = 32 units, habituated: n = 66 units, *P* = 0.55. (**L**) Left: Schematic illustrating the intersectional strategy to express ChRmine selectively in A1-targeting OFC neurons. Right: Coronal section showing the expression of ChRmine-oScarlet. (**M**) Raster (top) and peristimulus time histogram (bottom) of a representative single unit in A1. (**N**) Modulation Index of A1 L2/3 neural activity by transcranial photostimulation of OFC with a red laser. ChRmine: *n* = 6 mice, *P* = 0.012 (two-sided Wilcoxon signed-rank test). No opsin control: *n* = 3 mice, *P* = 0.67. ChRmine vs. no opsin: *P* = 0.034 (two-sided Wilcoxon rank-sum test).

function shared equally across frontal cortical areas. Alternatively, distinct frontal regions might apply unique filters on A1 activity, tailored to different types of predictions: OFC for predictions based on a history of experiences, and M2 for predictions related to motor corollary discharges.

To investigate these possibilities, we directly compared tone-evoked activities between OFCvl and M2 neurons within the same animals. We performed single-unit recordings using a Neuropixels 1.0 probe that penetrated both regions (Fig. 4I). When we compared tone responses between naïve and habituated mice, we found a 1.7-fold larger fraction of significantly excited OFCvl single units in habituated mice (habituated: 8.2%; naïve: 4.7%, *P* = 0.045), while M2 single-units showed no difference (habituated: 6.1%; naïve: 5.8%, *P* = 0.83) (Fig. 4J). Sound-evoked response magnitudes averaged across all excited single-units showed a significant increase after habituation in OFCvl (104% increase; *P* = 0.010; Fig. 4K). In contrast, M2 units showed a tendency for reduced activity, likely reflecting a weaker

304 input from the habituated auditory cortex (47% reduction; $P = 0.55$). Recordings in other frontal regions
305 also showed no signs of increased tone responses (fig. S8, A to F). This OFCvl-specific plasticity is
306 consistent with the OFCvl→A1 axonal imaging data and supports a division of labor between OFC and
307 M2 in the predictive filtering of A1 activity across different contexts.

308 To determine whether activation of the OFCvl→A1 pathway is sufficient to suppress A1 neuronal
309 activity, we next performed pathway-selective optogenetic activation. We restricted the expression of
310 red-shifted opsin ChRmine in A1-projecting OFCvl neurons by an intersectional viral approach (Fig.
311 4L). Transcranial illumination of the frontal cortex with a red laser successfully evoked action potentials
312 in ChRmine-expressing OFCvl neurons (fig. S8, G and H)(*62*, *63*). A1 recording during activation of
313 OFCvl→A1 pathway revealed significant suppression of A1 activity, an effect absent in control mice
314 without opsin expression (Modulation Index, ChRmine: -0.23 ± 0.06, $P = 0.012$; Control: 0.05 ± 0.07, P
315 $= 0.668$; ChRmine vs. Control: $P = 0.034$; Fig. 4, M and N). Together, these results indicate that the
316 OFCvl stores the information of repeated sensory stimuli and directly transmits predictive signals to A1,
317 triggering neural habituation in A1.

318 **Plasticity in SST cells amplifies sensory habituation**

319 Our results have demonstrated neural plasticity in the OFC, leading to the predictive filtering of A1
320 sensory responses. However, the OFC is considered to support flexible learning not only through its own
321 plasticity (*64–67*) but also by driving plasticity in other brain regions (*68–71*). A previous study found
322 that pairing OFC→A1 axon terminal activation with tone presentations results in plastic changes in A1
323 that suppress its responses to the paired frequency (*49*). Therefore, we wondered whether the enhanced
324 OFCvl→A1 input during habituation triggers synaptic plasticity in A1 to further amplify sensory
325 habituation.

326 We first explored the involvement of overall A1 synaptic plasticity in sensory habituation through
327 the area-selective knockout of N-methyl-D-aspartate (NMDA) receptors. We co-injected AAV9-
328 GCaMP6s and AAV8-mCherry-Cre into the A1 of floxed GluN1 mice (Grin1$^{flox/flox}$) (Fig. 5A). Previous
329 studies using the same mouse showed that Cre-dependent knockout of NMDA receptors became evident
330 within two weeks post-transfection and grew over subsequent weeks (*72–74*). Five weeks post-injection,
331 tone response magnitudes of A1 pyramidal cells were smaller in GluN1 knockout mice compared to
332 control mice (See Methods) (fig. S9, A to D), consistent with the loss of NMDA receptors. Comparing
333 five-day sensory habituation of GluN1 knockout mice to controls revealed a significant reduction in
334 across-day sensory habituation (Fig. 5B), suggesting that local synaptic plasticity in A1 amplifies long-
335 term sensory habituation.

336 Finally, we focused on synaptic plasticity specifically in SST cells. Given that GluN1 is also
337 expressed in SST cells and regulates their plasticity (*75*, *76*), we generated Grin1$^{flox/flox}$ mice carrying
338 SST-Cre to delete GluN1 selectively in SST cells. A1 pyramidal cells in these mice showed normal tone
339 response properties in a naïve condition (fig. S9, H to K). However, quantification of tone responses
340 across days revealed a significantly diminished habituation in SST cell GluN1 knockout mice compared
341 to the control group (Fig. 5, C and D). In contrast, selective deletion of GluN1 in VIP cells did not affect
342 sensory habituation (Fig. 5, E to G). Thus, while GluN1 deletion in SST cells does not alter basal sound
343 processing in A1, it attenuates sensory habituation through decreased synaptic plasticity. Collectively,
344 our experiments demonstrate that experience-dependent plasticity in both OFCvl circuits and A1 SST
345 cells leads to sensory habituation via the recruitment of SST inhibitory circuits by top-down predictive
346 signals.

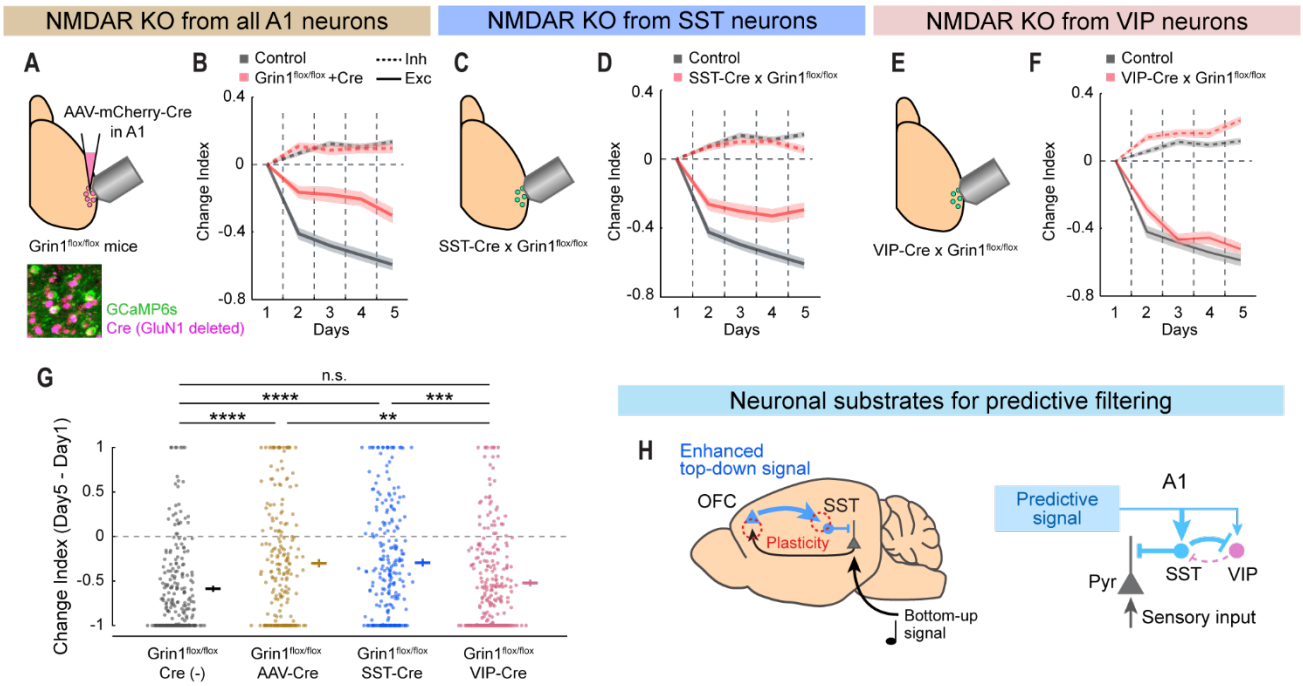

Fig. 5. NMDA receptors in A1 and SST cells are required for habituation. (**A**) Top: Schematic illustrating the viral strategy to knock out NMDA receptors in A1 neurons. Bottom: Representative two-photon image of A1 L2/3 neurons from a Grin1$^{flox/flox}$ mouse expressing GCaMP6s (green) and Cre (red). (**B**) Change Index for excitatory (solid line) and inhibitory (dotted line) sound-evoked responses across days in Grin1$^{flox/flox}$ (red) and control (black) mice. Grin1$^{flox/flox}$: n = 4 mice, 905 cells. Control: n = 5 mice, 1,708 cells. (**C-D**) Same as (a-b) but for knockout of NMDA receptors selectively in SST neurons. (**E**) SST-Cre × Grin1$^{flox/flox}$: n = 5 mice, 1,364 cells. Control: n = 6 mice, 1,740 cells. (**E-F**) Same as (a-b) but for knockout of NMDA receptors selectively in VIP neurons. (**F**) VIP-Cre × Grin1$^{flox/flox}$: n = 4 mice, 996 cells. Control: n = 5 mice, 1,494 cells. (**G**) Summary scatter plots showing the Change Index of excitatory responses in individual neurons on Day 5 compared to Day 1. Grin1$^{flox/flox}$, Cre^{-} control (Ctrl): n = 226 excited cells. Grin1$^{flox/flox}$ + AAV-Cre (KO_{A1}): n = 210. SST-Cre × Grin1$^{flox/flox}$ (KO_{SST}): n = 231. VIP-Cre × Grin1$^{flox/flox}$ (KO_{VIP}): n = 254. Ctrl vs. KO_{A1}: ****P = 6.9×10^{-5}. Ctrl vs. KO_{SST}: ****P = 3.2×10^{-7}. Ctrl vs. KO_{VIP}: P = 1.0. KO_{A1} vs. KO_{SST}: P = 1.0. KO_{A1} vs. KO_{VIP}: **P = 0.0034. KO_{SST} vs. KO_{VIP}: ***P = 3.2×10^{-4}. (two-sided Wilcoxon rank-sum test with Bonferroni correction). (**H**) Summary diagrams of sensory habituation pathways.

Discussion

Theories based on human psychophysics have suggested the role of internal predictive models in sensory habituation (fig. S1). Our findings identify the neural substrates for these predictive models and the negative images of sensory stimuli they generate. In naïve animals, bottom-up sensory signals evoke strong responses in the A1. However, with repeated exposure to the same sound over days, a predictive

368 model forms in the OFC. The OFC then sends top-down predictive signals to SST cells in the A1, which
369 in turn suppress the activity of pyramidal, VIP, and PV cells. This finding may appear at odds with the
370 focus of previous studies on the top-down regulation of VIP cells and the recruitment of the VIP→SST
371 disinhibitory circuit (*48*, *77*, *78*). However, quantification of cell type-specific retrograde tracing from
372 sensory cortical areas has revealed denser top-down connectivity from frontal cortical areas to SST than
373 VIP cells (*52*) (fig. S6). Furthermore, SST and VIP cells are known to form a mutual inhibitory loop
374 (*79–81*), with SST→VIP connections exhibiting one of the highest connection probabilities, largest IPSP
375 amplitudes, and strongest facilitation within cortical circuits (*82*). Therefore, it is not unexpected that
376 top-down input from OFCvl, which connects to both SST and VIP cells, could engage the often
377 overlooked SST→VIP inhibitory connection to suppress the A1 circuit. Synaptic plasticity in SST
378 neurons may further shift the balance of SST-VIP mutual inhibition toward SST dominance to facilitate
379 habituation (Fig. 5H). Our model successfully explains recent studies in V1 that identified a VIP-
380 dominant disinhibitory circuit during animals' first encounter with novel stimuli (*43*, *44*, *83*). We do not
381 exclude the roles of novelty or prediction error signals in other contexts (Supplementary Discussion).
382 However, our data indicate that daily sensory habituation is mediated by an increase in predictive
383 signals, rather than a decrease in novelty (prediction error) signals. Thus, plasticity in the OFC, through
384 the accumulation of experiences over extended periods (*64–67*), creates and updates the internal
385 predictive model of the sensory environment, which is then used to filter neural activity in sensory
386 cortices.

387 The OFC is considered to support flexible behaviors by encoding the values of predicted outcomes
388 (*84–86*), assigning prediction error credits to corresponding actions (*87*), and tracking associative
389 relationships between stimuli (*1*, *2*, *69*, *88*). However, the extent to which the OFC's top-down
390 projections influence sensory processing remains debated (*49*, *50*, *68*, *89*). Our finding of the OFC's role

391 in the predictive filtering of sensory inputs aligns with the concept that the OFC constructs and uses
392 internal associative models, or "cognitive maps," which dictate predictive relationships between the
393 sensory task space and possible outcomes (*1*, *2*). Furthermore, our results suggest a more generalized
394 function of the OFC beyond merely predicting explicitly rewarding or punishing action outcomes,
395 extending to the attenuation of salience in neutral stimuli during passive experiences. This broader role
396 is reminiscent of the OFC's involvement in "devaluation," where initially favorable stimuli lose their
397 value with satiety or new associations with unfavorable outcomes (*90–92*). It is plausible that sensory
398 inputs inherently carry behavioral values, as they may signal the approach of rewards or threats crucial
399 for an animal's survival. By forming internal associative models, the OFC "devalues" not only explicitly
400 rewarding stimuli but also neutral sensory inputs without meaningful outcomes, thereby inducing
401 habituation.

402 It is worth pointing out the similarity between our findings and the predictive filtering of self-
403 generated sounds, which has been proposed to involve the top-down pathway from the M2 to the A1
404 after days of movement-sound association (*53*, *54*). These studies suggested the recruitment of PV
405 inhibitory neurons, which broadly scale down the A1 activity during movements. Although exact circuits
406 are different, these findings collectively support a general principle: frontal cortical areas send top-down
407 predictive signals based on days of experience—M2 for movement-related predictions and the OFC for
408 familiarity-based predictions, respectively—to filter predictable sensory inputs. In support of this
409 division of labor, we observed a selective enhancement of sound-evoked activity in the OFC, but not in
410 M2, following sensory habituation. Aside from the predictive coding, previous studies also suggested
411 attentional filtering of A1 activity by the prefrontal cortex (*93–96*). Understanding how individual
412 frontal areas are recruited in specific contexts to apply these appropriate filters would be an important
413 area for future research.

Impaired habituation to repeated stimuli and resultant sensory hypersensitivity are commonly observed in mental disorders such as obsessive-compulsive disorders (*4*, *5*) and ASD (*7–10*). Although theories have proposed that a lack of predictive filtering may be central to the symptoms associated with ASD (*29–31*), the neural substrates linking altered neural wiring with reduced sensory filtering have remained unclear. Our discovery that top-down projections from the OFC to A1 are essential for auditory habituation provides crucial insights into the circuit mechanisms underlying reduced habituation in individuals with ASD. It is believed that the neocortical network in ASD displays long-range hypoconnectivity, as indicated by less cohesive activity across brain regions and reduced white matter volume (*97–100*). This reduced long-range communication between frontal areas and sensory cortices could therefore be a culprit for the insufficient habituation in these disorders. This general framework of top-down predictive filtering highlights the importance of targeting long-range frontal projections in developing interventions to alleviate sensory pathophysiology.

References:

1. R. Wilson, Y. Takahashi, G. Schoenbaum, Y. Niv, Orbitofrontal Cortex as a Cognitive Map of Task Space. Neuron 81, 267–279 (2014).
2. K. M. Costa, R. Scholz, K. Lloyd, P. Moreno-Castilla, M. P. H. Gardner, P. Dayan, G. Schoenbaum, The role of the lateral orbitofrontal cortex in creating cognitive maps. Nat. Neurosci. 26, 107–115 (2023).
3. N. C. Rust, M. R. Cohen, Priority coding in the visual system. Nat. Rev. Neurosci. 23, 376–388 (2022).
4. T. Y. Podoly, D. S. Derby, A. Ben-Sasson, Sensory over-responsivity and obsessive-compulsive

437 disorder: Measuring habituation and sensitivity through self-report, physiological and behavioral
438 indices. J. Psychiatr. Res. 149, 266–273 (2022).

439 5. M. Hallett, Tourette Syndrome: Update. Brain Dev. 37, 651–655 (2015).

440 6. D. Titone, T. Ditman, P. S. Holzman, H. Eichenbaum, D. L. Levy, Transitive inference in
441 schizophrenia: impairments in relational memory organization. Schizophr. Res. 68, 235–247
442 (2004).

443 7. J. A. Guiraud, E. Kushnerenko, P. Tomalski, K. Davies, H. Ribeiro, M. H. Johnson, Differential
444 habituation to repeated sounds in infants at high risk for autism. Neuroreport 22, 845–849 (2011).

445 8. S. A. Green, L. Hernandez, N. Tottenham, K. Krasileva, S. Y. Bookheimer, M. Dapretto,
446 Neurobiology of Sensory Overresponsivity in Youth With Autism Spectrum Disorders. JAMA
447 psychiatry 72, 778–786 (2015).

448 9. W. Jamal, A. Cardinaux, A. J. Haskins, M. Kjelgaard, P. Sinha, Reduced Sensory Habituation in
449 Autism and Its Correlation with Behavioral Measures. J. Autism Dev. Disord. 51, 3153–3164
450 (2021).

451 10. A. Kolesnik, J. Begum Ali, T. Gliga, J. Guiraud, T. Charman, M. H. Johnson, E. J. H. Jones,
452 Increased cortical reactivity to repeated tones at 8 months in infants with later ASD. Transl.
453 Psychiatry 9, 1–11 (2019).

454 11. C. H. Rankin, T. Abrams, R. J. Barry, S. Bhatnagar, D. F. Clayton, J. Colombo, G. Coppola, M. A.
455 Geyer, D. L. Glanzman, S. Marsland, F. K. McSweeney, D. A. Wilson, C. F. Wu, R. F. Thompson,
456 Habituation revisited: An updated and revised description of the behavioral characteristics of
457 habituation. Neurobiol. Learn. Mem. 92, 135–138 (2009).

458 12. R. F. Thompson, Habituation: a history. Neurobiol. Learn. Mem. 92, 127–134 (2009).

459 13. D. Wilson, C. Linster, Neurobiology of a simple memory. J. Neurophysiol. 100, 2–7 (2008).

460 14. M. Wehr, A. Zador, Synaptic mechanisms of forward suppression in rat auditory cortex. Neuron
461 47, 437–445 (2005).

462 15. R. G. Natan, J. J. Briguglio, L. Mwilambwe-Tshilobo, S. I. Jones, M. Aizenberg, E. M. Goldberg,
463 M. N. Geffen, Complementary control of sensory adaptation by two types of cortical
464 interneurons. Elife 4, e09868 (2015).

465 16. Y. Ayala, M. Malmierca, Cholinergic Modulation of Stimulus-Specific Adaptation in the Inferior
466 Colliculus. J. Neurosci. 35, 12261–12272 (2015).

467 17. V. Castellucci, H. Pinsker, I. Kupfermann, E. R. Kandel, Neuronal Mechanisms of Habituation
468 and Dishabituation of the Gill-Withdrawal Reflex in Aplysia. Science 167, 1745–1748 (1970).

469 18. F. M. Antunes, I. Nelken, E. Covey, M. S. Malmierca, Stimulus-Specific Adaptation in the
470 Auditory Thalamus of the Anesthetized Rat. PLoS One 5, e14071 (2010).

471 19. M. S. Malmierca, S. Cristaudo, D. Pérez-González, E. Covey, Stimulus-specific adaptation in the
472 inferior colliculus of the anesthetized rat. J. Neurosci. 29, 5483–5493 (2009).

473 20. N. Ulanovsky, L. Las, I. Nelken, Processing of low-probability sounds by cortical neurons. Nat.
474 Neurosci. 6, 391–398 (2003).

475 21. N. Ulanovsky, L. Las, D. Farkas, I. Nelken, Multiple time scales of adaptation in auditory cortex
476 neurons. J. Neurosci. 24, 10440–10453 (2004).

477 22. I. S. Westenberg, G. Paige, B. Golub, N. M. Weinberger, Evoked potential decrements in auditory
478 cortex. I. Discrete-trial and continual stimulation. Electroencephalogr. Clin. Neurophysiol. 40,
479 337–355 (1976).

480 23. I. S. Westenberg, N. M. Weinberger, Evoked potential decrements in auditory cortex. II. Critical
481 test for habituation. Electroencephalogr. Clin. Neurophysiol. 40, 356–369 (1976).

482 24. N. M. Weinberger, Associative representational plasticity in the auditory cortex: Resolving
483 conceptual and empirical problems. Debates Neurosci. 1, 85–98 (2007).

484 25. R. D. Hall, Habituation of evoked potentials in the rat under conditions of behavioral control.
485 Electroencephalogr. Clin. Neurophysiol. 24, 155–165 (1968).

486 26. S. F. Cooke, R. W. Komorowski, E. S. Kaplan, J. P. Gavornik, M. F. Bear, Visual recognition
487 memory, manifested as long-term habituation, requires synaptic plasticity in V1. Nat. Neurosci.
488 18, 262–271 (2015).

489 27. M. Ramaswami, Network Plasticity in Adaptive Filtering and Behavioral Habituation. Neuron 82,
490 1216–1229 (2014).

491 28. P. Sinha, M. M. Kjelgaard, T. K. Gandhi, K. Tsourides, A. L. Cardinaux, D. Pantazis, S. P.
492 Diamond, R. M. Held, Autism as a disorder of prediction. Proc. Natl. Acad. Sci. 111, 15220–

15225 (2014).

29. S. van de Cruys, K. Evers, R. van der Hallen, L. van Eylen, B. Boets, L. de-Wit, J. Wagemans, Precise minds in uncertain worlds: predictive coding in autism. Psychol. Rev. 121, 649–675 (2014).

30. H. Markram, T. Rinaldi, K. Markram, The intense world syndrome – an alternative hypothesis for autism. Front. Neurosci. 1, 77–96 (2007).

31. C. Moore, M. Carlen, U. Knoblich, J. Cardin, Neocortical Interneurons: From Diversity, Strength. Cell 142, 189–193 (2010).

32. K. Markram, H. Markram, The intense world theory - A unifying theory of the neurobiology of autism. Front. Hum. Neurosci. 4, 224 (2010).

33. M. Turatto, F. Bonetti, C. Chiandetti, D. Pascucci, Context-specific distractors rejection: contextual cues control long-term habituation of attentional capture by abrupt onsets. Vis. cogn. 27, 291–304 (2019).

34. W. P. Jordan, H. C. Strasser, L. McHale, Contextual control of long-term habituation in rats. J. Exp. Psychol. Anim. Behav. Process. 26, 323–339 (2000).

35. A. Dissegna, M. Turatto, C. Chiandetti, Context-specific habituation: A review. Animals 11, 1767 (2021).

36. H. K. Kato, M. W. Chu, J. S. Isaacson, T. Komiyama, Dynamic Sensory Representations in the Olfactory Bulb: Modulation by Wakefulness and Experience. Neuron 76, 962–975 (2012).

37. E. N. Sokolov, Higher nervous functions; the orienting reflex. Annu. Rev. Physiol. 25, 545–580 (1963).

38. C. Wacongne, J. P. Changeux, S. Dehaene, A Neuronal Model of Predictive Coding Accounting for the Mismatch Negativity. J. Neurosci. 32, 3665–3678 (2012).

39. A. R. Wagner, “Habituation and memory” in Mechanisms of Learning and Motivation, A. Dickinson, R. A. Boakes, Eds. (Psychology Press, Hillsdale, NJ, 1979).

40. H. K. Kato, S. N. Gillet, J. S. Isaacson, Flexible Sensory Representations in Auditory Cortex Driven by Behavioral Relevance. Neuron 88, 1027–1039 (2015).

41. S. N. Gillet, H. K. Kato, M. A. Justen, M. Lai, J. S. Isaacson, Fear Learning Regulates Cortical

Sensory Representations by Suppressing Habituation. Front. Neural Circuits 11, 112 (2018).

42. H. Makino, T. Komiyama, Learning enhances the relative impact of top-down processing in the visual cortex. Nat. Neurosci. 18, 1116–1122 (2015).

43. M. Garrett, S. Manavi, K. Roll, D. R. Ollerenshaw, P. A. Groblewski, N. D. Ponvert, J. T. Kiggins, L. Casal, K. Mace, A. Williford, A. Leon, X. Jia, P. Ledochowitsch, M. A. Buice, W. Wakeman, S. Mihalas, S. R. Olsen, Experience shapes activity dynamics and stimulus coding of VIP inhibitory cells. Elife 9, e50340 (2020).

44. M. Garrett, P. Groblewski, A. Piet, D. Ollerenshaw, F. Najafi, I. Yavorska, A. Amster, C. Bennett, M. Buice, S. Caldejon, L. Casal, F. D'Orazi, S. Daniel, S. E. de Vries, D. Kapner, J. Kiggins, J. Lecoq, P. Ledochowitsch, S. Manavi, N. Mei, C. B. Morrison, S. Naylor, N. Orlova, J. Perkins, N. Ponvert, C. Roll, S. Seid, D. Williams, A. Williford, R. Ahmed, D. Amine, Y. Billeh, C. Bowman, N. Cain, A. Cho, T. Dawe, M. Departee, M. Desoto, D. Feng, S. Gale, E. Gelfand, N. Gradis, C. Grasso, N. Hancock, B. Hu, R. Hytnen, X. Jia, T. Johnson, I. Kato, S. Kivikas, L. Kuan, Q. L'Heureux, S. Lambert, A. Leon, E. Liang, F. Long, K. Mace, I. M. de Abril, C. Mochizuki, C. Nayan, K. North, L. Ng, G. K. Ocker, M. Oliver, P. Rhoads, K. Ronellenfitch, K. Schelonka, J. Sevigny, D. Sullivan, B. Sutton, J. Swapp, T. K. Nguyen, X. Waughman, J. Wilkes, M. Wang, C. Farrell, W. Wakeman, H. Zeng, J. Phillips, S. Mihalas, A. Arkhipov, C. Koch, S. R. Olsen, Stimulus novelty uncovers coding diversity in visual cortical circuits. bioRxiv, 2023.02.14.528085 (2023).

45. K. Aitken, L. Campagnola, M. E. Garrett, S. R. Olsen, S. Mihalas, Simple synaptic modulations implement diverse novelty computations. Cell Rep. 43, 114188 (2024).

46. J. Homann, S. A. Koay, K. S. Chen, D. W. Tank, M. J. Berry, Novel stimuli evoke excess activity in the mouse primary visual cortex. Proc. Natl. Acad. Sci. U. S. A. 119, e2108882119 (2022).

47. D. P. Narayanan, H. Tsukano, A. M. Kline, K. Onodera, H. K. Kato, Biological constraints on stereotaxic targeting of functionally-defined cortical areas. Cereb. Cortex 33, 3293–3310 (2023).

48. S. Furutachi, A. D. Franklin, T. D. Mrsic-Flogel, S. B. Hofer, Cooperative thalamocortical circuit mechanism for sensory prediction errors. bioRxiv, 2023.07.12.548664 (2023).

49. D. E. Winkowski, D. A. Nagode, K. J. Donaldson, P. Yin, S. A. Shamma, J. B. Fritz, P. O. Kanold, Orbitofrontal Cortex Neurons Respond to Sound and Activate Primary Auditory Cortex Neurons.

Cereb. Cortex 28, 868–879 (2018).

50. D. Winkowski, S. Bandyopadhyay, S. Shamma, P. Kanold, Frontal Cortex Activation Causes Rapid Plasticity of Auditory Cortical Processing. J. Neurosci. 33, 18134–18148 (2013).

51. R. Ying, L. Hamlette, L. Nikoobakht, R. Balaji, N. Miko, M. L. Caras, Organization of orbitofrontal-auditory pathways in the Mongolian gerbil. J. Comp. Neurol. 531, 1459–1481 (2023).

52. G. ichi Tasaka, C. Maggi, E. Taha, A. Mizrahi, The local and long-range input landscape of inhibitory neurons in mouse auditory cortex. J. Comp. Neurol. 531, 502–514 (2023).

53. D. M. Schneider, J. Sundararajan, R. Mooney, A cortical filter that learns to suppress the acoustic consequences of movement. Nature 561, 391–395 (2018).

54. D. M. Schneider, A. Nelson, R. Mooney, A synaptic and circuit basis for corollary discharge in the auditory cortex. Nature 513, 189–194 (2014).

55. A. Nelson, D. Schneider, J. Takatoh, K. Sakurai, F. Wang, R. Mooney, A Circuit for Motor Cortical Modulation of Auditory Cortical Activity. J. Neurosci. 33, 14342–14353 (2013).

56. W. Sun, P. Tang, Y. Liang, J. Li, J. Feng, N. Zhang, D. Lu, J. He, X. Chen, The anterior cingulate cortex directly enhances auditory cortical responses in air-puffing-facilitated flight behavior. Cell Rep. 38, 110506 (2022).

57. S. W. Oh, J. A. Harris, L. Ng, B. Winslow, N. Cain, S. Mihalas, Q. Wang, C. Lau, L. Kuan, A. M. Henry, M. T. Mortrud, B. Ouellette, T. N. Nguyen, S. A. Sorensen, C. R. Slaughterbeck, W. Wakeman, Y. Li, D. Feng, A. Ho, E. Nicholas, K. E. Hirokawa, P. Bohn, K. M. Joines, H. Peng, M. J. Hawrylycz, J. W. Phillips, J. G. Hohmann, P. Wohnoutka, C. R. Gerfen, C. Koch, A. Bernard, C. Dang, A. R. Jones, H. Zeng, A mesoscale connectome of the mouse brain. Nature 508, 207–214 (2014).

58. Allen Institute for Brain Science, Allen Mouse Brain Connectivity Atlas (2011). http://connectivity.brain-map.org/.

59. L. Gao, S. Liu, L. Gou, Y. Hu, Y. Liu, L. Deng, D. Ma, H. Wang, Q. Yang, Z. Chen, D. Liu, S. Qiu, X. Wang, D. Wang, X. Wang, B. Ren, Q. Liu, T. Chen, X. Shi, H. Yao, C. Xu, C. T. Li, Y. Sun, A. Li, Q. Luo, H. Gong, N. Xu, J. Yan, Single-neuron projectome of mouse prefrontal cortex. Nat. Neurosci. 25, 515–529 (2022).

60. C. Cavada, T. Compañy, J. Tejedor, R. J. Cruz-Rizzolo, F. Reinoso-Suárez, The anatomical connections of the macaque monkey orbitofrontal cortex. A review. Cereb. Cortex 10, 220–242 (2000).

61. H. K. Srivastava, S. Bandyopadhyay, Parallel Lemniscal and Non-Lemniscal Sources Control Auditory Responses in the Orbitofrontal Cortex (OFC). eNeuro 7, 1–19 (2020).

62. R. Chen, F. Gore, Q. A. Nguyen, C. Ramakrishnan, S. Patel, S. H. Kim, M. Raffiee, Y. S. Kim, B. Hsueh, E. Krook-Magnusson, I. Soltesz, K. Deisseroth, Deep brain optogenetics without intracranial surgery. Nat. Biotechnol. 39, 161–164 (2021).

63. J. H. Marshel, Y. S. Kim, T. A. Machado, S. Quirin, B. Benson, J. Kadmon, C. Raja, A. Chibukhchyan, C. Ramakrishnan, M. Inoue, J. C. Shane, D. J. McKnight, S. Yoshizawa, H. E. Kato, S. Ganguli, K. Deisseroth, Cortical layer-specific critical dynamics triggering perception. Science 365, eaaw5202 (2019).

64. R. Hattori, N. G. Hedrick, A. Jain, S. Chen, H. You, M. Hattori, J. H. Choi, B. K. Lim, R. Yasuda, T. Komiyama, Meta-reinforcement learning via orbitofrontal cortex. Nat. Neurosci. 26, 2182–2191 (2023).

65. V. M. K. Namboodiri, J. M. Otis, K. van Heeswijk, E. S. Voets, R. A. Alghorazi, J. Rodriguez-Romaguera, S. Mihalas, G. D. Stuber, Single-cell activity tracking reveals that orbitofrontal neurons acquire and maintain a long-term memory to guide behavioral adaptation. Nat. Neurosci. 22, 1110–1121 (2019).

66. A. J. Whyte, H. W. Kietzman, A. M. Swanson, L. M. Butkovich, B. R. Barbee, G. J. Bassell, C. Gross, S. L. Gourley, A. contributions, S. designed research, S. performed research, S. analyzed data, N. Raj, J. Yamin, H. Arrowood, A. Allen, K. Zimmermann, Reward-related expectations trigger dendritic spine plasticity in the mouse ventrolateral orbitofrontal cortex. J. Neurosci. 39, 4595–4605 (2019).

67. C. M. Johnson, H. Peckler, L. H. Tai, L. Wilbrecht, Rule learning enhances structural plasticity of long-range axons in frontal cortex. Nat. Commun. 7, 1–14 (2016).

68. A. Banerjee, G. Parente, J. Teutsch, C. Lewis, F. F. Voigt, F. Helmchen, Value-guided remapping of sensory cortex by lateral orbitofrontal cortex. Nature 585, 245–250 (2020).

69. M. P. H. Gardner, G. Schoenbaum, The orbitofrontal cartographer. Behav. Neurosci. 135, 267–

608 276 (2021).

609 70. K. J. Miller, M. M. Botvinick, C. D. Brody, Value representations in the rodent orbitofrontal
610 cortex drive learning, not choice. Elife 11, e64575 (2022).

611 71. M. Malvaez, C. Shieh, M. D. Murphy, V. Y. Greenfield, K. M. Wassum, Distinct cortical–
612 amygdala projections drive reward value encoding and retrieval. Nat. Neurosci. 22, 762–769
613 (2019).

614 72. R. Deng, M. Chang, J. P. Y. Kao, P. O. Kanold, Cortical inhibitory but not excitatory synaptic
615 transmission and circuit refinement are altered after the deletion of NMDA receptors during early
616 development. Sci. Rep. 13, 656 (2023).

617 73. R. S. Larsen, I. T. Smith, J. Miriyala, J. E. Han, R. J. Corlew, S. L. Smith, B. D. Philpot, Synapse-
618 Specific Control of Experience-Dependent Plasticity by Presynaptic NMDA Receptors. Neuron
619 83, 879–893 (2014).

620 74. T. Iwasato, A. Datwani, A. M. Wolf, H. Nishiyama, Y. Taguchi, S. Tonegawa, T. Knöpfel, R. S.
621 Erzurumlu, S. Itohara, Cortex-restricted disruption of NMDAR1 impairs neuronal patterns in the
622 barrel cortex. Nature 406, 726–731 (2000).

623 75. M. Perez-Rando, E. Castillo-Gómez, R. Guirado, J. M. Blasco-Ibañez, C. Crespo, E. Varea, J.
624 Nacher, NMDA receptors regulate the structural plasticity of spines and axonal boutons in
625 hippocampal interneurons. Front. Cell. Neurosci. 11, 271022 (2017).

626 76. G. Nyíri, F. A. Stephenson, T. F. Freund, P. Somogyi, Large variability in synaptic n-methyl-d-
627 aspartate receptor density on interneurons and a comparison with pyramidal-cell spines in the rat
628 hippocampus. Neuroscience 119, 347–363 (2003).

629 77. Y. Fu, J. M. Tucciarone, J. S. Espinosa, N. Sheng, D. P. Darcy, R. A. Nicoll, Z. J. Huang, M. P.
630 Stryker, S. Espinosa, N. Sheng, D. P. Darcy, R. A. Nicoll, J. Huang, M. P. Stryker, A Cortical
631 Circuit for Gain Control by Behavioral State. Cell 156, 1139–1152 (2014).

632 78. S. Zhang, M. Xu, T. Kamigaki, J. P. H. Do, W.-C. Chang, S. Jenvay, K. Miyamichi, L. Luo, Y.
633 Dan, Long-range and local circuits for top-down modulation of visual cortex processing. Science
634 345, 660–665 (2014).

635 79. X. Jiang, S. Shen, C. R. Cadwell, P. Berens, F. Sinz, A. S. Ecker, S. Patel, A. S. Tolias, Principles
636 of connectivity among morphologically defined cell types in adult neocortex. Science 350,

aac9462 (2015).

80. C. K. Pfeffer, M. Xue, M. He, Z. J. Huang, M. Scanziani, Inhibition of inhibition in visual cortex: The logic of connections between molecularly distinct interneurons. Nat. Neurosci. 16, 1068–1076 (2013).

81. M. Karnani, J. Jackson, I. Ayzenshtat, J. Tucciarone, K. Manoocheri, W. Snider, R. Yuste, Cooperative Subnetworks of Molecularly Similar Interneurons in Mouse Neocortex. Neuron 90, 86–100 (2016).

82. L. Campagnola, S. C. Seeman, T. Chartrand, L. Kim, A. Hoggarth, C. Gamlin, S. Ito, J. Trinh, P. Davoudian, C. Radaelli, M. H. Kim, T. Hage, T. Braun, L. Alfiler, J. Andrade, P. Bohn, R. Dalley, A. Henry, S. Kebede, A. Mukora, D. Sandman, G. Williams, R. Larsen, C. Teeter, T. L. Daigle, K. Berry, N. Dotson, R. Enstrom, M. Gorham, M. Hupp, S. D. Lee, K. Ngo, P. R. Nicovich, L. Potekhina, S. Ransford, A. Gary, J. Goldy, D. McMillen, T. Pham, M. Tieu, L. Siverts, M. Walker, C. Farrell, M. Schroedter, C. Slaughterbeck, C. Cobb, R. Ellenbogen, R. P. Gwinn, C. D. Keene, A. L. Ko, J. G. Ojemann, D. L. Silbergeld, D. Carey, T. Casper, K. Crichton, M. Clark, N. Dee, L. Ellingwood, J. Gloe, M. Kroll, J. Sulc, H. Tung, K. Wadhwani, K. Brouner, T. Egdorf, M. Maxwell, M. McGraw, C. A. Pom, A. Ruiz, J. Bomben, D. Feng, N. Hejazinia, S. Shi, A. Szafer, W. Wakeman, J. Phillips, A. Bernard, L. Esposito, F. D. D'Orazi, S. Sunkin, K. Smith, B. Tasic, A. Arkhipov, S. Sorensen, E. Lein, C. Koch, G. Murphy, H. Zeng, T. Jarsky, Local connectivity and synaptic dynamics in mouse and human neocortex. Science 375, eabj5861 (2022).

83. K. Aitken, L. Campagnola, M. Garrett, S. Olsen, S. Mihalas, Familiarity modulated synapses model visual cortical circuit novelty responses. bioRxiv, 2023.08.16.553635 (2023).

84. C. Padoa-Schioppa, J. A. Assad, Neurons in the orbitofrontal cortex encode economic value. Nature 441, 223–226 (2006).

85. J. Hirokawa, A. Vaughan, P. Masset, T. Ott, A. Kepecs, Frontal cortex neuron types categorically encode single decision variables. Nature 576, 446–451 (2019).

86. G. Schoenbaum, A. A. Chiba, M. Gallagher, Orbitofrontal cortex and basolateral amygdala encode expected outcomes during learning. Nat. Neurosci. 1, 155–159 (1998).

87. M. E. Walton, T. E. J. Behrens, M. J. Buckley, P. H. Rudebeck, M. F. S. Rushworth, Separable learning systems in the macaque brain and the role of orbitofrontal cortex in contingent learning.

Neuron 65, 927–939 (2010).

88. G. Schoenbaum, M. R. Roesch, T. A. Stalnaker, Y. K. Takahashi, A new perspective on the role of the orbitofrontal cortex in adaptive behaviour. Nat. Rev. Neurosci. 10, 885–892 (2009).

89. D. Liu, J. Deng, Z. Zhang, Z. Y. Zhang, Y. G. Sun, T. Yang, H. Yao, Orbitofrontal control of visual cortex gain promotes visual associative learning. Nat. Commun. 11, 1–14 (2020).

90. J. D. Howard, T. Kahnt, Identity-Specific Reward Representations in Orbitofrontal Cortex Are Modulated by Selective Devaluation. J. Neurosci. 37, 2627–2638 (2017).

91. M. P. H. Gardner, J. S. Conroy, M. H. Shaham, C. V. Styer, G. Schoenbaum, Lateral Orbitofrontal Inactivation Dissociates Devaluation-Sensitive Behavior and Economic Choice. Neuron 96, 1192-1203.e4 (2017).

92. J. A. Gottfried, J. O'Doherty, R. J. Dolan, Encoding predictive reward value in human amygdala and orbitofrontal cortex. Science 301, 1104–1107 (2003).

93. M. Nakajima, L. I. Schmitt, M. M. Halassa, Prefrontal Cortex Regulates Sensory Filtering through a Basal Ganglia-to-Thalamus Pathway. Neuron 103, 445-458.e10 (2019).

94. J. Fritz, S. Shamma, M. Elhilali, D. Klein, Rapid task-related plasticity of spectrotemporal receptive fields in primary auditory cortex. Nat. Neurosci. 6, 1216–1223 (2003).

95. J. B. Fritz, M. Elhilali, S. A. Shamma, Differential dynamic plasticity of A1 receptive fields during multiple spectral tasks. J. Neurosci. 25, 7623–7635 (2005).

96. J. Fritz, M. Elhilali, S. Shamma, Adaptive changes in cortical receptive fields induced by attention to complex sounds. J. Neurophysiol. 98, 2337–2346 (2007).

97. M. E. Vissers, M. X Cohen, H. M. Geurts, Brain connectivity and high functioning autism: A promising path of research that needs refined models, methodological convergence, and stronger behavioral links. Neurosci. Biobehav. Rev. 36, 604–625 (2012).

98. J. J. Wolff, H. Gu, G. Gerig, J. T. Elison, M. Styner, S. Gouttard, K. N. Botteron, S. R. Dager, G. Dawson, A. M. Estes, A. C. Evans, H. C. Hazlett, P. Kostopoulos, R. C. McKinstry, S. J. Paterson, R. T. Schultz, L. Zwaigenbaum, J. Piven, Differences in white matter fiber tract development present from 6 to 24 months in infants with autism. Am. J. Psychiatry 169, 589–600 (2012).

99. E. Courchesne, K. Pierce, Why the frontal cortex in autism might be talking only to itself: Local

694 over-connectivity but long-distance disconnection. Curr. Opin. Neurobiol. 15, 225–230 (2005).

695 100. S. Wass, Distortions and disconnections: Disrupted brain connectivity in autism. Brain Cogn. 75,
696 18–28 (2011).

697 101. M. Pachitariu, C. Stringer, M. Dipoppa, S. Schröder, L. F. Rossi, H. Dalgleish, M. Carandini, K.
698 D. Harris, Suite2p: beyond 10,000 neurons with standard two-photon microscopy. bioRxiv,
699 061507 (2017).

700 102. M. Pachitariu, N. Steinmetz, S. Kadir, M. Carandini, K. D. Harris, Kilosort: realtime spike-sorting
701 for extracellular electrophysiology with hundreds of channels. bioRxiv, 061481 (2016).

702 103. C. Rossant, S. Kadir, D. Goodman, J. Schulman, M. Hunter, A. Saleem, A. Grosmark, M.
703 Belluscio, G. Denfield, A. Ecker, A. Tolias, S. Solomon, G. Buzsaki, M. Carandini, K. Harris,
704 Spike sorting for large, dense electrode arrays. Nat Neurosci 19, 634–641 (2016).

705 104. J. M. J. Fabre, E. H. van Beest, A. J. Peters, M. Carandini, K. D. Harris, Bombcell: automated
706 curation and cell classification of spike-sorted electrophysiology data. Zenodo, doi:
707 10.5281/ZENODO.8172822 (2023).

708 105. Y. Senzai, A. Fernandez-Ruiz, G. Buzsáki, Layer-Specific Physiological Features and
709 Interlaminar Interactions in the Primary Visual Cortex of the Mouse. Neuron 101, 500-513.e5
710 (2019).

711 106. I. Wickersham, D. Lyon, R. Barnard, T. Mori, S. Finke, K.-K. Conzelmann, J. Young, E.
712 Callaway, Monosynaptic Restriction of Transsynaptic Tracing from Single, Genetically Targeted
713 Neurons. Neuron 53, 639–647 (2007).

714 107. T. Moser, D. Beutner, Kinetics of exocytosis and endocytosis at the cochlear inner hair cell
715 afferent synapse of the mouse. Proc. Natl. Acad. Sci. U. S. A. 97, 883–888 (2000).

716 108. J. D. Goutman, Mechanisms of synaptic depression at the hair cell ribbon synapse that support
717 auditory nerve function. Proc. Natl. Acad. Sci. U. S. A. 114, 9719–9724 (2017).

718 109. K. Meyer, E. M. Rouiller, G. Loquet, Direct comparison between properties of adaptation of the
719 auditory nerve and the ventral cochlear nucleus in response to repetitive clicks. Hear. Res. 228,
720 144–155 (2007).

721 110. G. Loquet, E. M. Rouiller, Neural adaptation to pulsatile acoustical stimulation in the cochlear

nucleus of the rat. Hear. Res. 171, 72–81 (2002).

111. D. Duque, X. Wang, J. Nieto-Diego, K. Krumbholz, M. S. Malmierca, Neurons in the inferior colliculus of the rat show stimulus-specific adaptation for frequency, but not for intensity. Sci. Rep. 6, 1–15 (2016).

112. G. G. Parras, J. Nieto-Diego, G. V. Carbajal, C. Valdés-Baizabal, C. Escera, M. S. Malmierca, Neurons along the auditory pathway exhibit a hierarchical organization of prediction error. Nat. Commun. 8, 1–17 (2017).

113. L. A. Anderson, G. B. Christianson, J. F. Linden, Stimulus-specific adaptation occurs in the auditory thalamus. J. Neurosci. 29, 7359–7363 (2009).

114. R. G. Natan, W. Rao, M. N. Geffen, Cortical Interneurons Differentially Shape Frequency Tuning following Adaptation. Cell Rep. 21, 878–890 (2017).

115. G. Keller, T. Bonhoeffer, M. Hübener, Sensorimotor Mismatch Signals in Primary Visual Cortex of the Behaving Mouse. Neuron 74, 809–815 (2012).

116. N. J. Audette, W. X. Zhou, A. La Chioma, D. M. Schneider, Precise movement-based predictions in the mouse auditory cortex. Curr. Biol. 32, 4925-4940.e6 (2022).

117. R. Näätänen, A. W. K. Gaillard, S. Mäntysalo, Early selective-attention effect on evoked potential reinterpreted. Acta Psychol. (Amst). 42, 313–329 (1978).

118. A. M. H. Lesicko, C. F. Angeloni, J. M. Blackwell, M. De Biasi, M. N. Geffen, Cortico-Fugal Regulation of Predictive Coding. Elife 11, e73289 (2022).

119. K. Obara, T. Ebina, S. I. Terada, T. Uka, M. Komatsu, M. Takaji, A. Watakabe, K. Kobayashi, Y. Masamizu, H. Mizukami, T. Yamamori, K. Kasai, M. Matsuzaki, Change detection in the primate auditory cortex through feedback of prediction error signals. Nat. Commun. 14, 1–17 (2023).

120. A. Hockley, M. S. Malmierca, Auditory processing control by the medial prefrontal cortex: A review of the rodent functional organisation. Hear. Res. 443, 108954 (2024).

121. J. H. Sul, H. Kim, N. Huh, D. Lee, M. W. Jung, Distinct Roles of Rodent Orbitofrontal and Medial Prefrontal Cortex in Decision Making. Neuron 66, 449–460 (2010).

122. J. P. O'Doherty, P. Dayan, K. Friston, H. Critchley, R. J. Dolan, Temporal Difference Models and Reward-Related Learning in the Human Brain. Neuron 38, 329–337 (2003).

123. A. C. Nobre, J. T. Coull, C. D. Frith, M. M. Mesulam, Orbitofrontal cortex is activated during breaches of expectation in tasks of visual attention. Nat. Neurosci. 2, 11–12 (1999).

124. S. W. Kennerley, A. F. Dahmubed, A. H. Lara, J. D. Wallis, Neurons in the Frontal Lobe Encode the Value of Multiple Decision Variables. J. Cogn. Neurosci. 21, 1162–1178 (2009).

125. Y. K. Takahashi, M. R. Roesch, T. A. Stalnaker, R. Z. Haney, D. J. Calu, A. R. Taylor, K. A. Burke, G. Schoenbaum, The Orbitofrontal Cortex and Ventral Tegmental Area Are Necessary for Learning from Unexpected Outcomes. Neuron 62, 269–280 (2009).

126. T. A. Stalnaker, T. L. Liu, Y. K. Takahashi, G. Schoenbaum, Orbitofrontal neurons signal reward predictions, not reward prediction errors. Neurobiol. Learn. Mem. 153, 137–143 (2018).

127. F. Pouille, M. Scanziani, Routing of spike series by dynamic circuits in the hippocampus. Nature 429, 717–723 (2004).

Acknowledgments: We thank Paul Manis, Jeffry Isaacson, Daniel Polley, and the members of the Kato Lab for their advice throughout the project and comments on the manuscript. We thank Gonçalo Lopes for his support in setting up Bonsai for pupil monitoring.

Funding:

National Institutes of Health grant R01DC017516 (HKK)
National Institute of Health grant RF1NS128873 (HKK)
Simons Foundation (HKK)
Eagles Autism Foundation (HKK)
Foundation of Hope (HKK, HT).

Author contributions:

Conceptualization: HT, HKK
Methodology: HT, MMG, HKK
Investigation: HT, MMG, PRD, HKK
Formal analysis: HT, HKK
Visualization: HT, HKK
Funding acquisition: HT, HKK

Project administration: HKK

Supervision: HKK

Writing – original draft: HT, HKK

Writing – review & editing: HT, MMG, PRD, HKK

Competing interests: The authors declare no competing interests.

Data and materials availability: All data generated in this study will be deposited in the DANDI Archive. Source data for all figures will be provided in this paper as a supplementary data file attached to this paper. Custom Matlab codes used in this study will be made available from the corresponding author upon request.